

The momentum space electronic structure and the charge order of high temperature $\text{Ca}_{2-x}\text{Na}_x\text{CuO}_2\text{Cl}_2$ and $\text{Bi}_2\text{Sr}_2\text{CaCu}_2\text{O}_{8+\delta}$ superconductors

Jian-Qiao Meng,¹ M. Brunner,¹ K.-H. Kim,² H.-G. Lee,² S.-I. Lee,²
J. S. Wen,³ Z. J. Xu,³ G. D. Gu,³ and G.-H. Gweon^{1,*}

¹*Department of Physics, University of California, Santa Cruz, CA 95064, USA*

²*Department of Physics, Pohang University of Science and Technology, Pohang 790784, South Korea*

³*Condensed Matter Physics and Materials Science Department,
Brookhaven National Laboratory, Upton, New York 11973, USA*

(Dated: April 25, 2022)

We study the electronic structure of $\text{Ca}_{2-x}\text{Na}_x\text{CuO}_2\text{Cl}_2$ and $\text{Bi}_2\text{Sr}_2\text{CaCu}_2\text{O}_{8+\delta}$ samples in a wide range of doping, using angle-resolved photoemission spectroscopy, with emphasis on the Fermi surface (FS) in the near anti-nodal region. The “nesting wave vector,” i.e., the wave vector that connects two nearly flat pieces of the FS in the anti-nodal region, reveals a universal monotonic decrease in magnitude as a function of doping. Comparing our results to the charge order recently observed by scanning tunneling spectroscopy (STS), we conclude that the FS nesting and the charge order pattern seen in STS do not have a direct relationship. Therefore, the charge order likely arises due to strong correlation physics rather than FS nesting physics.

PACS numbers: 74.25.Jb,71.18.+y,74.72.-h,79.60.-i

The origin of the “pseudo-gap” remains a central mystery in the physics of high-temperature superconductors. The pseudo-gap [1, 2] means that the single-particle spectral function $A(\vec{k}, \omega)$ shows depleted spectral weight at the Fermi energy (E_F) in the metallic phase above the superconducting transition temperature, in stark contrast to a Landau quasi-particle peak at E_F that is expected for a normal Fermi liquid. By now, the pseudo-gap is routinely observed by experimental tools that probe $A(\vec{k}, \omega)$, the angle-resolved photoelectron spectroscopy (ARPES) or, its Fourier transform, the scanning tunneling spectroscopy (STS).

Recently, quite a few ARPES and STS studies [3–10] have contributed to an emerging phenomenology of the pseudo-gap. In this emerging picture, the pseudo-gap is separate from the superconducting gap, is dominant in the “anti-nodal” region in the momentum space, and is characterized by a “checkerboard pattern” of charge order in the real space. In particular, this checkerboard pattern, representing an organization of the electron density with approximately four lattice constant periodicities along the a or b direction of the (nearly) tetragonal CuO_2 lattice, is observed in all the samples of cuprates that have been found to be appropriate for STS studies, i.e., $\text{Bi}_2\text{Sr}_2\text{CaCu}_2\text{O}_{8+\delta}$ (Bi2212) compounds [11–16], $\text{Bi}_{2-y}\text{Pb}_y\text{Sr}_{2-z}\text{La}_z\text{CuO}_{6+\delta}$ (Bi2201) compounds [17], and $\text{Ca}_{2-x}\text{Na}_x\text{CuO}_2\text{Cl}_2$ (Na-CCOC) compounds [9, 18]. This unique feature, while strong in the underdoped regime, is observed up to near-optimal doping [11] or optimal doping [9], albeit with a diminished weight.

What is the underlying mechanism of the checkerboard pattern? Here we shall differentiate between two generic scenarios, a weak-correlation scenario and a strong-correlation scenario. In the first scenario, we associate the checkerboard pattern as reflecting the instability of

the electron system due to a Fermi-surface (FS) nesting. Thus, here we are envisioning the standard Peierls-type charge-density-wave (CDW) phenomenon [19] or the standard weak-coupling spin-density-wave (SDW) phenomenon [20]. In the second scenario, we consider the checkerboard pattern as driven by large-energy scale physics, as opposed to the FS nesting physics. For instance, the checkerboard pattern has been attributed to an instability of the Hubbard model [21], or to the formation of a Wigner solid of hole pairs embedded in a sea of d -wave resonating valence bond (RVB) states [22]. The essential criterion by which we can distinguish the two mechanisms is the agreement between the Fermi-surface nesting wave vector and the checkerboard periodicity. Within the second scenario, this agreement is not a required primary feature but an optional feature. Within the first scenario, this agreement is an absolute requirement.

In our definition above, we take the weak-correlation FS-based scenario as the FS nesting scenario only, leaving out other, generally possible, one-electron-band mechanisms such as the van Hove singularity-induced CDW [23]. Note also that a FS object such as the “Fermi arc” [24] may give rise to a high Lindhard susceptibility due to the high density of states at extremal points of the arc, causing a CDW. Such a Fermi-arc-based CDW scenario, e.g., as suggested in a recent STS work [10], requires a fundamental modification of the FS to a Fermi arc with a strong correlation as a *prerequisite* and does *not* involve FS nesting. Thus, such a scenario should be considered as a strong-correlation scenario, not as a weak correlation scenario.

Thus, we pose the subsequent question: For high-temperature superconductors, is there a direct connection between the Fermi-surface nesting and the checker-

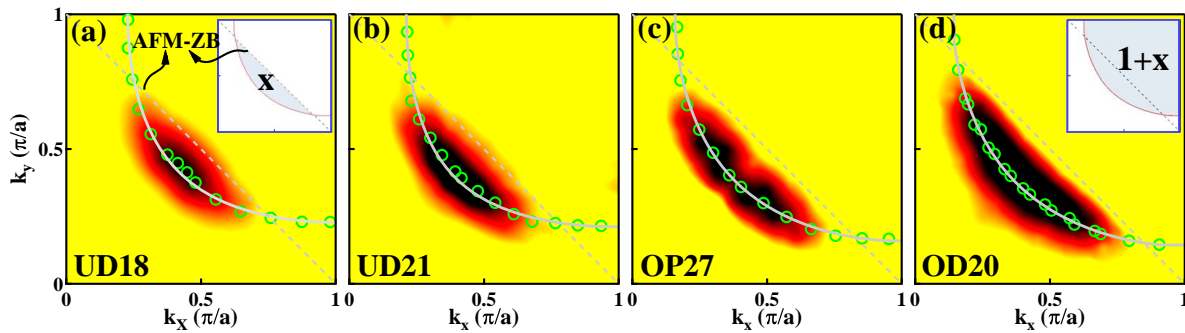


FIG. 1. (Color online) Doping evolution of the Fermi energy intensity maps for (a) UD18, (b) UD21, (c) OP27, and (d) OD20 Na-CCOC samples. The energy integration window $[-10 \text{ meV}, +10 \text{ meV}]$ centered at E_F was used. These maps are obtained by symmetrizing the original data with respect to the $(0,0)-(\pi,\pi)$ line. The Fermi momentum values determined by the maximum of the MDC at E_F are marked by open circles (green). The solid lines (gray) show fits to the Fermi surface of the tight-binding band theory [28]. In the color map, dark (black) means high intensity and pale (yellow) means low intensity. The insets of (a), and (d) are discussed later (“Luttinger sum rule”).

board pattern? A survey of the literature does not give a clear answer, which this paper now aims to provide. One does find in the literature, however, some initial attempts at such an answer. For example, a recent work on Bi2201 superconductors [17] found that the periodicity of the charge order pattern is a strong function of the doping, ranging from 4.5 lattice constants in the underdoped region to 6.2 lattice constants at the optimal doping. Qualitatively, this trend is what one would expect for a weak-correlation scenario, as the authors of that work have indeed suggested. In addition, this conclusion appears to be supported by work on Na-CCOC compounds, where a good agreement between the Fermi-surface nesting vector in ARPES [25] and the checkerboard periodicity [18] has been noted. However, this study was limited to low doping values, and in view of more recent work [9], a study covering a wider doping range including optimal doping is necessary to attain a firm conclusion.

In this paper, we report ARPES data on Na-CCOC samples and Bi2212 samples in view of these questions. We significantly widen the doping range of the Na-CCOC samples studied by ARPES in comparison to previous studies [25, 26], and find that such an improvement is of essential importance. We compare our results on Na-CCOC and Bi2212 samples with their known checkerboard periodicity values. We re-examine the degree of agreement, or disagreement, between the Fermi-surface nesting and the checkerboard pattern for Na-CCOC samples, and, in addition, Bi2201 samples. We find that in all the cases examined, such an agreement is absent, or accidental at best. Thus, we find that a strong-correlation scenario is much more likely than a weak-correlation scenario for explaining the pseudo-gap.

The photoemission measurements were carried out at beam line 5-4 of the Stanford Synchrotron Radiation

Lightsource (SSRL) and at beam line 10.0.1 of the Advanced Light Source (ALS) at Lawrence Berkeley National Laboratory, using a Scienta R4000 electron energy analyzer. The photon energy used was 25.5 eV for Na-CCOC and 25 eV for Bi2212, both with an energy resolution of 15-20 meV. The angular resolution is $\sim 0.2^\circ$ (0.008 \AA^{-1} in momentum). Na-CCOC samples, grown by a high-pressure flux method to unprecedented high doping values for this experiment, include underdoped samples ($T_c = 18, \text{ and } 21 \text{ K}$), optimally doped samples ($T_c = 27 \text{ K}$), and overdoped samples ($T_c = 20 \text{ K}$) [27]. Bi2212 samples were grown by the traveling solvent floating-zone method, and include underdoped samples ($T_c = 74 \text{ K}$), optimally doped samples ($T_c = 91 \text{ K}$), and overdoped samples ($T_c = 74 \text{ K}$). Hereafter, we will refer to the samples with the usual “ T_c notation” such as UD74, OP91, and OD74, where UD, OP, and OD mean under-doping, optimal doping and overdoping, respectively. All samples were cleaved *in situ* and measured in an ultra-high vacuum with a base pressure of better than 4×10^{-11} mbar. For Na-CCOC samples measurements were made at 10 K, while for Bi2212 samples measurements were made at 200 K for UD74 and OP91 samples, and at 100 K for OD74 samples. It is worth noting that recent advances [9, 27] in high-pressure sample growth resulted in the accessibility of the optimally doped and overdoped samples of the Na-CCOC samples, for which no ARPES data have been reported previously to our knowledge.

Figure 1 shows ARPES intensity maps at E_F for Na-CCOC samples. While these data were taken at 10 K in the superconducting phase, the data will be discussed here only in terms of the Fermi arc [24] and the pseudo-gap, with the more elusive and weaker feature of the superconductivity left for a possible future study [9, 25, 29].

This figure clearly shows that the high-intensity re-

gion of the map (“Fermi arc” [24]) increases its length as a function of doping, as expected. From our data, we define, operationally, the “Fermi surface” as the contour determined by the momentum distribution curve (MDC) peak positions (circle symbols). These Fermi surfaces in Figs. 1(a), and 1(b) are in good agreement with those published previously on the same compounds with similar doping values [25].

Figure 2(a) shows the energy distribution curves (EDCs) near the anti-nodal point, as a function of doping. It is seen that these EDCs are characterized by a large pseudo-gap, with the weight at E_F strongly suppressed. This is quite reminiscent of a large pseudo-gap and the lack of a coherent peak, as reported by STS [9].

Figure 2(c) shows the MDCs for a cut at the anti-nodal point for the UD21 sample, and Fig 2(d) for the OP27 sample. In Figs. 1(c) and 2(d), MDCs are fit with two Lorentzian curves (red dashed lines) and the positions

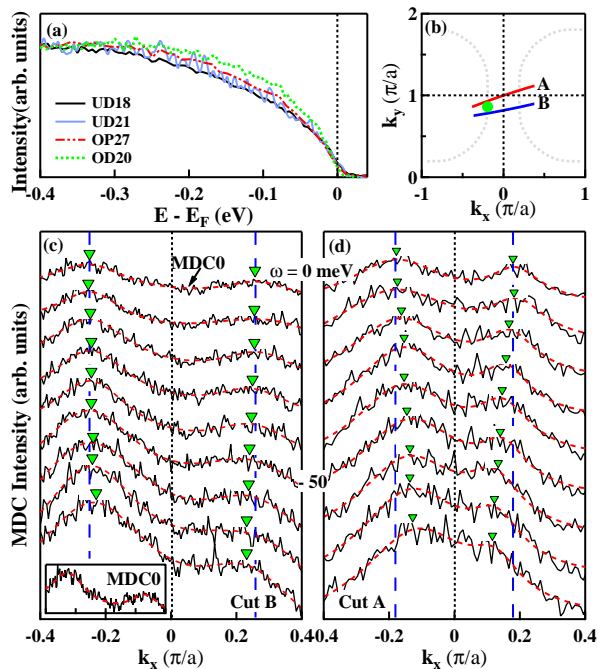


FIG. 2. (Color online) (a) EDCs in the anti-nodal region [see (b) for the \vec{k} information], as a function of doping for Na-CCOC. (b) \vec{k} space cuts A,B corresponding to the data of (d), and (c), respectively, and the approximate \vec{k} value (point) corresponding to the data of (a). (c), and (d) MDCs as a function of the binding energy for UD21 (c) and OP27 (d). Red dashed lines are fit curves (see text) and the vertical dashed lines (blue) correspond to the peak positions at $\omega = 0$, i.e. at E_F . The curves are separated vertically for easy view, and the binding energy values for adjacent curves differ by 10 meV. The inset of (c) re-displays the E_F data, emphasizing the clear two peak structure. The two peaks for each curve are marked by triangular symbols, each of which indicates both the peak position and its uncertainty (horizontal size) as determined by the MDC fit procedure.

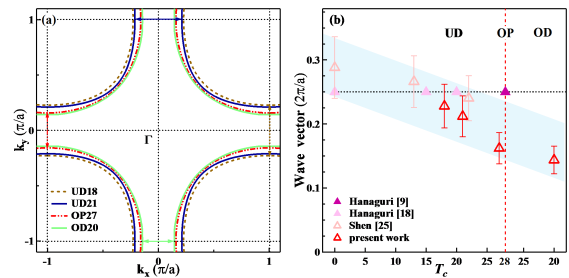


FIG. 3. (Color online) (a) “Fermi surfaces” as a function of doping for Na-CCOC, corresponding to the data of Fig. 1. The arrows indicate the nesting vectors. (b) FS nesting vectors (open symbols) and STS wave vectors (filled symbols). The vertical dashed line (red) indicates the position of $T_{c,max}$.

of the two Lorentzian peaks are marked with triangle symbols. In agreement with a previous work [25], the MDCs for the underdoped sample do not show appreciable dispersion up to a binding energy of ~ 50 meV. However, the MDCs for the optimally doped sample show clear dispersions at a binding energy of $\gtrsim 30$ meV. This is consistent with the known qualitative behavior of the pseudo-gap as a function of doping [30].

The Fermi surface as defined in Fig. 1 becomes flat as it crosses the Brillouin zone boundary. Thus the Fermi surface near the anti-nodal point is approximately nested, as observed previously [25], and the nesting vector can be determined from our Fermi surfaces. This is shown in Fig. 3(a), which summarizes all of our Fermi surfaces of Fig. 1.

Figure 3(b) summarizes our nesting wave vectors, along with the wave vectors corresponding to the checkerboard patterns of STS [9, 18]. Also, included in the figure are the nesting wave vectors determined for underdoped samples of Na-CCOC by Shen *et al.* [25]. First of all, it can be easily noted that our data agree well with Shen *et al.*’s data for the overlapping doping region. Second, our data, now extended to optimal doping and overdoping, clearly indicate that the nesting vector is a decreasing function of doping. Third, in hindsight, the data by Shen *et al.* also show the same trend. Fourth, for the optimal doping, the FS nesting would imply a CDW periodicity that is too large ($\gtrsim 5.5a$) as compared with the checkerboard periodicity ($4a$).

Previously [25] the agreement between the ARPES nesting vector and the checkerboard wave vector was interpreted to be very important. Given our findings above, however, there emerges another possibility; The nesting wave vector and the checkerboard periodicity are independent, although they might coincide by accident. This is suggested by the striking disagreement found in the doping dependence and a similarly striking disagreement in the value at optimal doping, although the second can be considered as a mere consequence of the first.

In order to help determine which case is more likely, we

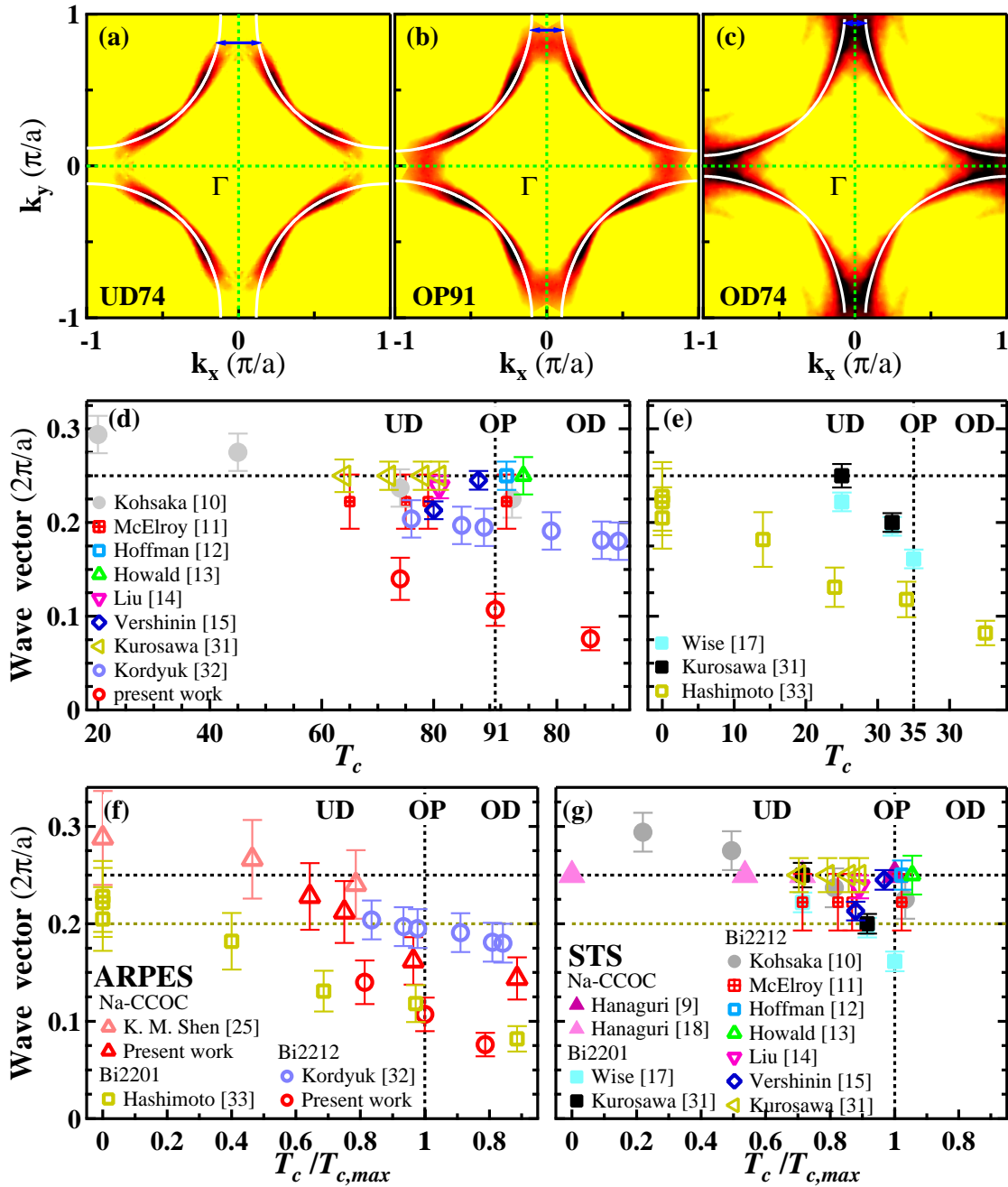


FIG. 4. (Color online) (a)-(c) Normal-state Fermi energy intensity maps of Bi2212. White lines show fits to the Fermi surface of the tight-binding band theory [28]. (d) The FS nesting vectors and the STS charge order wave vectors for Bi2212, from this work and from the literature [10–15, 31, 32]. (e) Similar plot for Bi2201 samples. All data are from the literature [17, 31, 33]. The formats of (d) or (e) are similar to those of Fig.3(b). (f), (g) Summary of all ARPES nesting vectors (f) and STS charge order wave vectors (g), showing their overall contrasting behaviors.

now discuss Bi2212 superconductors and Bi2201 superconductors. Fig. 4(a)-(c) show ARPES intensity maps for Bi2212 samples. Fig. 4(d) summarizes the comparison of STS data and ARPES data for Bi2212. The main feature is that the Fermi-surface nesting vector for Bi2212 is always too small in comparison with the checkerboard

wave vectors. Our experimental data show the behavior of the anti-bonding band dispersion, while the data of Kordyuk *et al.* [32], included in Fig. (d), emphasize the behavior of the bonding band dispersion, consistent with the well-known empirical band structure of Bi2212 [28]. The STS data on Bi2212 suggest that the checkerboard

periodicity is 3.5 - 4.5 lattice constants, while the FS nesting would predict ≈ 5 , or much greater, lattice constants. Clearly, Fig. 4(d) points out the difficulty of reconciling the ARPES data with the STS data in the presence of bilayer splitting, a point that has been already raised in a different context [34].

Figure 4(e) shows the comparison for Bi2201 superconductors. ARPES and STS disagree greatly here also. Furthermore, the disagreement becomes *greater* as doping decreases, i.e., as the pseudo-gap physics becomes more important. A related observation is as follows: While the doping dependence of the STS data is in qualitative agreement with that of the ARPES data, as pointed out previously [17], the slope of the STS data is actually ≈ 2.5 times too large in magnitude, as Fig. 4(e) shows.

Finally, Fig. 4(f), and 4(g) present all the data of Fig. 3(b),4(d), and 4(e) in a different way. The wave vectors are plotted as a function of normalized T_c 's. Two main discrepancies between ARPES and STS are observed. First, ARPES data show a universal slope, while STS data do not. Second, STS wave vectors show a narrow distribution, with most values belonging in the range [0.2, 0.25], while ARPES data show a wide and uniform distribution.

Putting aside this summary of discrepancies between ARPES and STS, one might ask "is there a way to understand the apparent complexity in the data of Bi2212 [Fig. 4(d)]?" The presence of bilayer splitting in the ARPES data and the mixed trends of the doping dependence in the STS data, the latter presumably being due to different conditions of STS experiments, contribute to this apparent complexity. Fig. 4(f), which shows good agreement between the bonding (anti-bonding) band data for Bi2212 with the data for Na-CCOC (Bi2201), might be viewed as suggesting a possible picture where the kinds of discrepancies observed in Na-CCOC [Fig. 3(b)] and Bi2201 [Fig. 4(e)] have a mixed presence in Bi2212, giving rise to the observed complexity.

To sum up, a weak-coupling CDW (or SDW) scenario is highly unlikely. Instead a strong-electron correlation is likely the driving force of the charge order. Note that this conclusion does not rule out the possibility of a cooperative or secondary effect of the FS nesting or a similar momentum-space mechanism [10].

Our claim is corroborated by more evidence. First, if the FS nesting is the driving force, then it is difficult to explain why the underdoping region is preferred for the charge order. According to a previous study on Bi2212 [32], the FS in the anti-nodal region becomes very flat, and thus more highly nesting, at overdoping. Second, the FS nesting scenario would require that the checkerboard pattern reverses the contrast as the sample bias voltage changes sign [35]. The STS data [9] show quite the opposite: The contrast is nonreversal.

The consideration of the so-called "Luttinger sum rule"

[36] provides general additional support. The sum rule concerns x , the hole doping per unit cell. In a strong correlation scenario, the sum rule is satisfied only by the combination of the Luttinger surface (LS) and the FS. We follow the theory of Ref. [36], and take the LS to be the anti-ferromagnetic zone boundary (AFM-ZB) and the FS to be approximately the geometry formed by the Fermi arc and the AFM-ZB. As indicated in the inset of Fig. 1(a), in this scenario, the FS accounts for only x . In a weak-correlation scenario, the FS is now large, and accounts for $1 + x$, as indicated in Fig. 1(d). Assuming the strong-correlation scenario, then, we obtain $x = 0.11, 0.16, 0.21$, and 0.23 , respectively from UD18 through OD20. In the weak-correlation scenario, $x = 0.00, 0.06, 0.15$, and 0.19 . So, while the latter scenario may be appropriate for optimal or over doping, it fails completely at underdoping. Our sum-rule analysis here agrees well with a similar analysis based on the STS data of Bi2212 [10], where a connection between the modified FS in the strong correlation scenario and charge order was noted, as already discussed above, and also with a recent ARPES work on Bi2212 [37].

To conclude, the electron correlation is of *primary* importance for the charge order and the pseudo-gap in cuprates. In electron-correlation-based scenarios, the checkerboard periodicity has been shown to be doping independent [21], as in Na-CCOC, or an argument based on the domain size has been given [22] to explain the small doping dependence seen in Bi2212. In closing, we note that similar strong-correlation-based charge order scenarios have been proposed recently for quasi-one-dimensional cuprates [38] and La-based superconductors [39], motivating further work.

G.H.G. acknowledges helpful discussions with S. A. Kivelson and D.-H. Lee. G.H.G. and J.Q.M thank K. M. Shen for helpful discussions. The work at UCSC was supported partially by a COR FRG grant. Portions of this research were carried out at the Stanford Synchrotron Radiation Lightsource (SSRL), a Directorate of SLAC National Accelerator Laboratory and an Office of Science User Facility operated for the U.S. Department of Energy Office of Science by Stanford University. The Advanced Light Source (ALS) is supported by the Director, Office of Science, Office of Basic Energy Sciences, of the U.S. Department of Energy under Contract No. DE-AC02-05CH11231. The work at the BNL was supported by DOE under Contract No. DE-AC02-98CH10886.

* Corresponding author: gweon@ucsc.edu

- [1] H. Ding, T. Yokoya, J. C. Campuzano, T. Takahashi, M. Randeria, M. R. Norman, T. Mochiku, K. Kadowaki, and J. Giapintzakis, Nature (London) **382**, 51 (1996).
- [2] T. Timusk, and B. Statt, Rep. Prog. Phys. **62**, 61(1999).
- [3] K. Tanaka, W. S. Lee, D. H. Lu, A. Fujimori, T. Fujii,

- Risdiana, I. Terasaki, D. J. Scalapino, T. P. Devereaux, Z. Hussain, and Z.-X. Shen, *Science* **314**, 1910 (2006).
- [4] T. Kondo, T. Takeuchi, A. Kaminski, S. Tsuda, and S. Shin, *Phys. Rev. Lett.* **98**, 267004 (2007).
- [5] W. S. Lee, I. M. Vishik, K. Tanaka, D. H. Lu, T. Sasagawa, N. Nagaosa, T. P. Devereaux, Z. Hussain, and Z.-X. Shen, *Nature(London)* **450**, 81 (2007).
- [6] K. Terashima, H. Matsui, T. Sato, T. Takahashi, M. Kofu, and K. Hirota, *Phys. Rev. Lett.* **99**, 017003 (2007).
- [7] T. Kondo, R. Khasanov, T. Takeuchi, J. Schmalian, and A. Kaminski, *Nature(London)* **457**, 296 (2009).
- [8] M. C. Boyer, W. D. Wise, K. Chatterjee, M. Yi, T. Kondo, T. Takeuchi, H. Ikuta and E. W. Hudson, *Nat. Phys.* **3**, 802 (2007).
- [9] T. Hanaguri, Y. Kohsaka, J. C. Davis, C. Lupien, I. Yamada, M. Azuma, M. Takano, K. Ohishi, M. Ono, and H. Takagi, *Nat. Phys.* **3**, 865 (2007).
- [10] Y. Kohsaka, C. Taylor, P. Wahl, A. Schmidt, Jinhwan Lee, K. Fujita, J. W. Alldredge, K. McElroy, Jinho Lee, H. Eisaki, S. Uchida, D.-H. Lee, and J. C. Davis, *Nature(London)* **454**, 1072 (2008).
- [11] K. McElroy, D.-H. Lee, J. E. Hoffman, K. M. Lang, J. Lee, E. W. Hudson, H. Eisaki, S. Uchida, and J. C. Davis, *Phys. Rev. Lett.* **94** 197005 (2005).
- [12] J. E. Hoffman, E. W. Hudson, K. M. Lang, V. Madhavan, H. Eisaki, S. Uchida, and J. C. Davis, *Science* **295**,466(2002).
- [13] C. Howald, H. Eisaki, N. Kaneko, M. Greven, and A. Kapitulnik, *Phys. Rev. B* **67**, 014533 (2003).
- [14] Y. H. Liu, K. Takeyama, T. Kurosawa, N. Momono, M. Oda, and M. Ido, *Phys. Rev. B* **75**, 212507 (2007).
- [15] M. Vershinin, S. Misra, S. Ono, Y. Abe, Yoichi Ando, and A. Yazdani, *Science* **303**, 1995 (2004).
- [16] C. Howald, H. Eisaki, N. Kaneko, and A. Kapitulnik, *Proc. Natl. Acad. Sci. (U.S.A)* **100**, 9705 (2003).
- [17] W. D. Wise, M. C. Boyer, K. Chatterjee, T. Kondo, T. Takeuchi, H. Ikuta, Yayu Wang, and E. W. Hudson, *Nat. Phys.* **4**, 696 (2008).
- [18] T. Hanaguri, C. Lupien, Y. Kohsaka, D.-H. Lee, M. Azuma, M. Takano, H. Takagi, and J. C. Davis, *Nature (London)* **430**, 1001 (2004).
- [19] R. E. Peierls, *Quantum Theory of Solids* (Oxford University Press, New York, 1955), p. 108.
- [20] G. Grüner, *Density Waves in Solids*, (Addison-Wesley, Reading, MA, 1994).
- [21] G. Seibold, J. Lorenzana, and M. Grilli, *Phys. Rev. B* **75**, 100505(R) (2007).
- [22] P. W. Anderson, cond-mat/0406038.
- [23] T.M. Rice and G.K. Scott, *Phys. Rev. Lett.* **35**, 120 (1975).
- [24] M. R. Norman, H. Ding, M. Randeria, J. C. Campuzano, T. Yokoya, T. Takeuchi, T. Takahashi, T. Mochiku, K. Kadowaki, P. Guptasarma, and D. G. Hinks, *Nature(London)* **392**, 157 (1998).
- [25] K. M. Shen, F. Ronning, D. H. Lu, F. Baumberger, N. J. C. Ingle, W. S. Lee, W. Meevasana, Y. Kohsaka, M. Azuma, M. Takano, H. Takagi, and Z.-X. Shen, *Science* **307**, 901 (2005).
- [26] T. Sasagawa, F. Ronning, Y. Kohsaka, K. M. Shen, T. Yoshida, M. Azuma, M. Takano, Z.-X. Shen, and H. Takagi, *Physica C* **388-389**, 307 (2003).
- [27] K.-H. Kim, H.-J Kim, J.-D Kim, and H.-G. Lee, *Journal of the Korean Physical Society.* **48**, 1032 (2006).
- [28] R. S. Markiewicz, S. Sahrakorpi, M. Lindroos, Hsin Lin, and A. Bansil, *Phys. Rev. B* **72**, 054519 (2005).
- [29] A possible feature in our data to be associated with the superconductivity is a few meV shift of the leading edge for the spectra within the Fermi arc. Given the energy window used in our experiment, this is a minor feature that needs further investigation.
- [30] A. Damascelli, Z. Hussain, and Z.-X. Shen, *Rev. Mod. Phys.* **75**, 473 (2003).
- [31] T. Kurosawa, T. Yoneyama, Y. Takano, M. Hagiwara, R. Inoue, N. Hagiwara, K. Kurusu, K. Takeyama, N. Momono, M. Oda, and M. Ido, *Phys. Rev. B* **81**, 094519 (2010); A. Hashimoto, N. Momono, M. Oda, and M. Ido, *ibid* **74**, 064508 (2006).
- [32] A. A. Kordyuk, S. V. Borisenko, M. S. Golden, S. Legner, K. A. Nenkov, M. Knupfer, J. Fink, H. Berger, L. Forro, and R. Follath, *Phys. Rev. B* **66**, 014502 (2002).
- [33] M. Hashimoto, T. Yoshida, H. Yagi, M. Takizawa, A. Fujimori, M. Kubota, K. Ono, K. Tanaka, D. H. Lu, Z.-X. Shen, S. Ono, and Yoichi Ando, *Phys. Rev. B* **77**, 094516 (2008).
- [34] R. S. Markiewicz, *Phys. Rev. B* **69**, 214517 (2004).
- [35] P. Mallet, K. M. Zimmermann, Ph. Chevalier, J. Marcus, J. Y. Veullen, and J. M. Gomez Rodriguez, *Phys. Rev. B* **60**, 2122 (1999).
- [36] Kai-Yu Yang, T. M. Rice, and Fu-Chun Zhang, *Phys. Rev. B* **73**, 174501 (2006).
- [37] H.-B. Yang, J. D. Rameau, Z.-H. Pan, G. D. Gu, P. D. Johnson, H. Claus, D. G. Hinks, and T. E. Kidd, *Phys. Rev. Lett.* **107**, 047003 (2011).
- [38] A. Rusydi, W. Ku, B. Schulz, R. Rauer, I. Mahns, D. Qi, X. Gao, A. T. S. Wee, P. Abbamonte, H. Eisaki, Y. Fujimaki, S. Uchida, and M. Rbhausen, *Phys. Rev. Lett.* **105**, 026402 (2010).
- [39] E. Berg, E. Fradkin, S. A Kivelson, and J. M Tranquada, *New Journal of Physics* **11**, 115004 (2009).